Int. J. Heat Mass Transfer. Vol. 34, No. 4/5, pp. 1113–1124, 1991
Printed in Great Britain

0017-9310/91 $3.00+0.00

Evaporative cooling of liquid film through interfacial heat and mass transfer in a vertical channel—II. Numerical study

W. M. YAN and T. F. LIN
Department of Mechanical Engineering, National Chiao Tung University, Hsinchu, Taiwan 30050, R.O.C.

(*Received* 9 *August* 1989 *and in final form* 18 *June* 1990)

Abstract—A numerical analysis is carried out to investigate the evaporative cooling of liquid falling film through interfacial heat and mass transfer in natural convection channel flows. Results for heat and mass transfer rates are specifically presented for the systems with ethanol film evaporation. The predicted results are also contrasted with the experimental results. The predictions show that the effects of the evaporative latent heat transfer on the cooling of the liquid film depend largely on the inlet liquid film temperature and liquid mass flow rate. Additionally, the results indicate that the heat transfer from the interface to the gas stream is predominated by the transport of the latent heat in conjunction with the liquid film evaporation.

1. INTRODUCTION

MOMENTUM, mass and thermal interactions between the falling liquid films along the vertical channel surface and the gas/vapour stream are widely encountered in industrial applications. In the present study the main concerns are to investigate the importance of the latent heat transport associated with the evaporation of the falling liquid film in the buoyancy-driven flows and to extend this concept to the cooling of the electronic system and the design of the natural type of cooling towers.

Due to the miniaturization of electronic circuitry, the cooling of electronic equipment especially in VLSI devices becomes more and more important. Since the dissipated heat in VLSI devices would rise to a level as high as 10^5 W m^{-2} [1], thermal engineers must face the challenge of removing high flux by means of any efficient heat transfer modes—natural or forced convection, conduction, or phase change—while maintaining relatively low component temperature. In order to achieve even higher heat transfer rates, the use of liquid–vapour phase change in the form of liquid film vaporization is one of the promising methods [2]. This is just one of the applications of film evaporation.

Another prominent application of the vaporization of the liquid film is in the cooling tower (evaporative cooler). The cooling tower generally consists of large chambers loosely filled with trays. Water to be cooled is pumped to the top of the tower, where it is distributed by sprays or tray troughs. It then falls through the tower, splashing down from duct to duct. As the water droplets fall down, a part of them evaporates into the air flow which is induced by the chimney effect of the warm humid air in the tower. The enthalpy needed for the evaporation is taken from the water. Therefore, the water is cooled. The chimney effect, namely the flow driven through a vertical channel by the buoyancy actions, could be greatly enhanced if the water to be cooled is directed to flow down over the vertical surfaces of the chamber. This is the co-called natural type of cooling tower because in it no external mechanical force is required.

In analysing the problem under investigation the momentum, heat and mass transfer in the gas flow and liquid film must be simultaneously considered with the appropriate treatment of the gas–liquid interface. Since the gas stream induced by the combined buoyancy forces of thermal and mass diffusion along with the shear force acted by the falling film could move upwards or downwards and the shape of the gas–liquid interface is quite complex, the influence of the finite liquid film on the heat and mass transfer in the gas flow is difficult to assess without the help of the experimental study. A combined theoretical and experimental study on heat and mass transfer in buoyancy-driven flows with a finite-liquid film was conducted. In this article, only the theoretical results are presented to investigate the evaporative cooling of a liquid falling film through interfacial heat and mass transfer in a natural convection channel flow. As for the experimental study, the experimental results were presented in the related work [3]. Due to the space limit, the detailed literature review is omitted and is available in the related work [3]. Now we are in a position to present the remaining parts of this study. In Section 2, the numerical algorithm is developed. The wave model accounting for the effects of the interfacial waves on the transport phenomena in both gas stream and liquid film is proposed in Section 3. In Section 4, the solution method is presented. The

NOMENCLATURE

B	liquid mass flow rate per unit periphery length at inlet
b	half channel width
c_p	specific heat
c_{pa}	specific heat for air
c_{pv}	specific heat for vapour
D	mass diffusivity
$\tilde{D}$	wave mass diffusivity
d_g	damping function in gas side
d_l	damping function in liquid side
f	wave frequency
Gr_M	Grashof number (mass transfer), $g(M_a/M_v-1)(w_l-w_o)b^4/lv_o^2$
Gr_T	Grashof number (heat transfer), $g(T_l-T_o)b^4/(lv_o^2T_o)$
g	gravitational acceleration
h_{fg}	latent heat of vaporization
l	channel length
$\dot{m}_l''$	interfacial mass flux
M_a	molecular weight of air
M_r	dimensionless accumulated evaporation rate
M_v	molecular weight of vapour
Nu_x	interfacial local Nusselt number
p	mixture pressure
p_l	partial pressure of vapour at gas–liquid interface
p_m	motion pressure (dynamic pressure), $p-p_o$
Pr	Prandtl number of the mixture
Pr_l	Prandtl number of the liquid film
q_l''	total interfacial energy flux in gas side
q_{ll}''	interfacial latent heat flux in gas side (or net enthalpy flux), $\dot{m}_l''h_{fg}$
q_{sl}''	interfacial sensible heat flux in gas side, $[(\lambda+\tilde{\lambda})\partial T/\partial y]_{g,l}$
Re_{li}	liquid film Reynolds number
Sc	Schmidt number
Sh	interfacial local Sherwood number
T	temperature
T_l	gas–liquid interface temperature
T_{li}	inlet liquid film temperature
T_w	wall temperature
u	axial velocity
u_l	gas–liquid interface velocity
u_o	inlet axial velocity
v	transverse velocity
w	mass fraction of vapour
w_l	mass fraction of vapour at gas–liquid interface, equation (17)
We	Weber number, equation (23)
x	coordinate in the flow direction
y	coordinate in the transverse direction.

Greek symbols

Γ	dimensionless surface tension parameter, equation (24a)
δ	local liquid film thickness
δ'	average wave amplitude
λ	molecular thermal conductivity
$\tilde{\lambda}$	wave thermal conductivity
μ	molecular dynamic viscosity
$\tilde{\mu}$	wave dynamic viscosity
ρ	density
τ_l	shear force at the gas–liquid interface.

Subscripts

a	air
g	mixture (air+ethanol vapour)
I	condition at the gas–liquid interface
l	liquid film
o	ambient condition or inlet condition
v	vapour
w	condition of wall.

results of numerical prediction are discussed in great detail in Section 5. Finally, concluding remarks are drawn in Section 6.

2. ANALYSIS

The geometry of the system to be examined, as schematically shown in Fig. 1, is the vertical parallel plates with channel height l and half channel width b. The channel walls are wetted by thin liquid films with an inlet liquid temperature T_{li}. The channel walls are insulated in order to investigate the evaporative cooling, associated with the latent heat transport of film vaporization. Because strong evaporation of the liquid film occurs at the gas–liquid interface, the energy required to sustain the evaporation must largely come from the internal energy of the liquid film, which then experiences a reduction in temperature. Hence, the heat and mass transfer occurs as the liquid film falls down the channel surface. Meanwhile, the induced flow in the gas side results due to the combined buoyancy forces of thermal and mass diffusion together with the shear force acted by the falling film. Therefore, momentum, heat and mass transfer in both the liquid film and gas flow should be simultaneously analysed.

To make the problem tractable by the boundary-layer analysis, only the cases in which the induced gas flow is in downward direction are chosen to examine the effects of the transport processes in finite liquid film on film evaporation in natural convection channel flows. The detailed description about the flow reversal and the justification of the boundary-layer assumptions are available in refs. [4, 5]. With this selection,

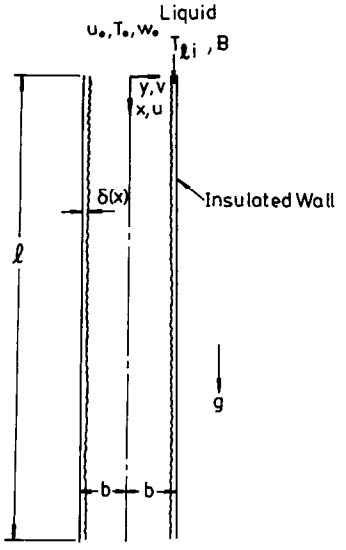

FIG. 1. Schematic diagram of the physical system.

the buoyancy induced heat and mass transfer in a vertical channel can then be treated by the boundary-layer analysis.

2.1. *Governing equations*

2.1.1. *Liquid film.* As a preliminary study consideration is given to a system with low liquid mass flow rate and hence the liquid film is assumed to flow laminarly. To facilitate the analysis, the inertia term in the momentum equation for the liquid film is neglected [6, 7], for it is small compared with the diffusional term (viscous term). Therefore, the two-dimensional boundary-layer flow in the fluid film is governed by the following conservation equations:

axial-momentum equation

$$0 = \frac{\partial}{\partial y}\left[(\mu_l + \tilde{\mu}_l)\frac{\partial u_l}{\partial y}\right] + \rho_l g, \tag{1}$$

energy equation

$$\rho_l c_{pl} u_l \frac{\partial T_l}{\partial x} = \frac{\partial}{\partial y}\left[(\lambda_l + \tilde{\lambda}_l)\frac{\partial T_l}{\partial y}\right] \tag{2}$$

where $\tilde{\mu}_l$ and $\tilde{\lambda}_l$ are the wave viscosity and wave conductivity due to the interfacial wave effects which will be modelled in Section 3.

2.1.2. *Gas flow.* The steady natural convection flows resulting from the combined buoyancy effects of thermal and mass diffusion can be described by the basic equations as:

continuity equation

$$\frac{\partial}{\partial x}(\rho u) + \frac{\partial}{\partial y}(\rho v) = 0, \tag{3}$$

axial-momentum equation

$$\rho u\frac{\partial u}{\partial x} + \rho v\frac{\partial u}{\partial y} = -\frac{\mathrm{d}p_m}{\mathrm{d}x} + \frac{\partial}{\partial y}\left[(\mu + \tilde{\mu})\frac{\partial u}{\partial y}\right] + g(\rho - \rho_o), \tag{4}$$

energy equation

$$\rho c_p u\frac{\partial T}{\partial x} + \rho c_p v\frac{\partial T}{\partial y} = \frac{\partial}{\partial y}\left[(\lambda + \tilde{\lambda})\frac{\partial T}{\partial y}\right] + \rho(D + \tilde{D})(c_{pv} - c_{pa})\frac{\partial T}{\partial y}\frac{\partial w}{\partial y}, \tag{5}$$

concentration equation

$$\rho u\frac{\partial w}{\partial x} + \rho v\frac{\partial w}{\partial y} = \frac{\partial}{\partial y}\left[\rho(D + \tilde{D})\frac{\partial w}{\partial y}\right] \tag{6}$$

where $\tilde{\mu}$, $\tilde{\lambda}$, and $\tilde{D}$ are respectively the wave viscosity, wave conductivity and wave mass diffusivity, which account for the effects of the interfacial waves on the transport processes in the gas flow. Note that in the present study the thermophysical properties are taken to be variable. The detailed evaluation of them is given in refs. [4, 8].

2.2. *Boundary conditions*

At the inlet the flow is in the x-direction with uniform velocity, temperature and mass fraction profiles:

$$x = 0: \quad u = u_o, \quad T = T_o, \quad w = w_o, \quad p_m = -\rho u_o^2/2. \tag{7}$$

The condition at the centreline of the channel is

$$y = 0: \quad \frac{\partial u}{\partial y} = 0, \quad \frac{\partial T}{\partial y} = 0, \quad \frac{\partial w}{\partial y} = 0. \tag{8}$$

The conditions at the gas–liquid interface are

$$y = b - \delta(x): \quad u = u_l(x), \quad T = T_l(x), \quad w = w_l(x). \tag{9}$$

The conditions at the channel wall are

$$y = b: \quad u_l = 0, \quad \partial T_l/\partial y = 0. \tag{10}$$

The condition at the exit is

$$x = l: \quad p_m = 0. \tag{11}$$

It should be mentioned here that the pressure defects at the inlet and exit are determined by the equations $p_m = -\rho_o u_o^2$ and 0, respectively. Strictly speaking, pressure conditions at the inlet and exit should be determined by a complete analysis, including not only the flow in the channel but also the flows in the immediate surroundings around the inlet and exit. This would greatly complicate the analysis and is beyond the scope of the present study. But it is noted that as far as the heat and mass transfer characteristics are concerned, the boundary-layer type of analysis performed here is satisfactory in practical applications [9, 10].

2.3. *Interfacial balances*

To make the problem tractable, the interface is assumed to be smooth. But the effects of the interfacial wave motion is accounted for by introducing the wave properties, $\tilde{\mu}$, $\tilde{\lambda}$, and $\tilde{D}$ into the boundary conditions and differential equations. The interfacial balances are described as follows:

velocity

$$u_l = (u)_{l,I} = (u)_{g,I}, \tag{12}$$

temperature

$$T_l = (T)_{l,I} = (T)_{g,I}, \tag{13}$$

shear stress

$$\tau_l = [(\mu+\tilde{\mu})(\partial u/\partial y)]_{l,I} = [(\mu+\tilde{\mu})(\partial u/\partial y)]_{g,I}, \tag{14}$$

mass balance

$$\dot{m}_l'' = [\rho(D+\tilde{D})/(1-w_l)]\cdot(\partial w/\partial y)_l, \tag{15}$$

energy balance

$$[(\lambda+\tilde{\lambda})(\partial T/\partial y)]_{l,I} = [(\lambda+\tilde{\lambda})(\partial T/\partial y)]_{g,I}+\dot{m}_l''\cdot h_{fg}. \tag{16}$$

It is noted that in equation (16) the terms on the right-hand side represent the interfacial sensible heat flux from the interface to the gas stream q_{sI}'' and the net enthalpy flux to the interface due to latent heat transfer (film vaporization) q_{lI}'', respectively. The term on the left-hand side of equation (16) stands for the interfacial heat flux in the liquid side and is regarded as the total interfacial heat flux, $q_l''(=q_{sI}''+q_{lI}'')$.

The interfacial mass fraction is obtained by assuming the gas–liquid interface to be in thermodynamic equilibrium [4, 5]

$$w_l = M_v p_l/[M_a(p-p_l)+M_v p_l]. \tag{17}$$

3. WAVE MODEL

When the falling liquid film is disturbed so that the fluid particles are displaced from their original streamlines, two kinds of resulting forces, gravity and surface tension, can be called into play. The motion of the fluid brought by these restoring forces will not cease when the fluid particle has reached its original position of dynamic equilibrium but will overshoot the mark and requires the action of the restoring forces again. Thus wave motion is generated.

The surface waves on a falling liquid film normally appear at $Re_{li} > 20$ except for regions near the start of the flow. The waves appearing at the line of wave inception have a two-dimensional character with roughly sinusoidal-like wave fronts moving down the surface. These sinusoidal-like waves persist for a short distance but soon begin to distort. In the region of flow immediately following the sinusoidal-like wave, there are significant spatial variations in wavelength and dispersion characteristics [11].

Due to the complexity of the characteristics of wave motion, very few works have directly considered the influence of the interfacial waves on the transfer processes. To account for the effects of wave motion on the heat and mass transfer, a simple wave model for $\tilde{\mu}$ in parallel with the Prandtl–Kolmogorof hypothesis [12] is used. The wave viscosity for the liquid film is expressed as [12]

$$\tilde{\mu}_l = c_l \rho_l \delta'^2 f d_l \tag{18}$$

where δ' is the wave amplitude and f the wave frequency. Since the wave-induced motion is damped out near the channel wall, a damping function d_l is used to set $\tilde{\mu}_l$ to zero near the channel wall.

The wave-induced motion is also expected to affect the gas flow near the interface. The effects are taken into account by introducing a wave viscosity $\tilde{\mu}_g$ defined as

$$\tilde{\mu}_g = c_g \rho_g \delta'^2 f d_g \tag{19}$$

where the values for c_l and c_g are respectively chosen to be 0.1 and 10 so as to make the magnitudes of the wave dynamic viscosities for the liquid and gas phases to be approximately equal to 10% of the corresponding molecular viscosity for each phase and to make the predicted results confirm to the general perception that the existence of the interfacial wave can augment the heat and mass transfer rates by 10–20%. In the gas flow, a damping function d_g is also employed. In the present study the damping functions, d_l and d_g, are optimized via a number of test runs. The detailed description is available in ref. [4]. The damping functions d_l and d_g are

$$d_l = 1-\exp[-(b-y)/\delta] \tag{20a}$$

and

$$d_g = \exp[-5(b-\delta-y)/\delta]. \tag{20b}$$

During the test runs, it is found that as the constants c_g and c_l are chosen to be zero (i.e. the effects of the wavy interface on the gas and liquid phases are neglected entirely), the predicted heat transfer rates in the gas stream are underpredicted by about 10–20%. The detailed description is available in ref. [4].

Since no systematical study of the wave parameters for the ethanol falling film exists in literature, the theoretical data of the wave parameters obtained by Hirshburg and Florschuetz [13] for the water falling film are used. Empirical relations for the wave frequency f and wave amplitude δ' fitting their theoretical results are

$$\begin{aligned} f &= 86.7We^{0.371327}(\mathrm{s}^{-1}), && \text{if } We \leqslant 0.0264443 \\ &= 71.79We^{0.319413}(\mathrm{s}^{-1}), && \text{if } We > 0.0264443 \end{aligned} \tag{21}$$

and

$$\begin{aligned} \delta' &= 4.1236\times10^{-4}We^{0.5505}(\mathrm{m}), && \text{if } We \leqslant 0.038357 \\ &= 1.5340\times10^{-4}We^{0.2472}(\mathrm{m}), && \text{if } We > 0.038357 \end{aligned} \tag{22}$$

where the Weber number, We, is defined as

$$We = (Re_{li}/4)^{5/3}/\Gamma \tag{23}$$

where the surface tension parameter Γ and liquid film Reynolds number Re_{li} are defined as

$$\Gamma = 0.6736219(\sigma/\rho_l v_l^{4/3}) \tag{24a}$$

and

$$Re_{li} = 4B/\mu_l. \tag{24b}$$

In the above equation B is the liquid mass flow rate per unit periphery length at the inlet and σ the surface tension of the liquid film. The temperature dependence of the surface tension for ethanol is available in refs. [4, 8].

It should be emphasized that in the present study the Weber number has been assumed to be the governing dimensionless group for the falling film waves. Therefore, the wave parameters of the ethanol falling film can be approximately estimated from those of the water falling film. This assumption was verified by the theoretical results of Massot *et al.* [14] and Gollan and Sideman [15].

Notice that the wave properties, $\tilde{\lambda}$ and $\tilde{D}$, are estimated by introducing the wave Prandtl number $\tilde{Pr}$ and wave Schmidt number $\tilde{Sc}$. In the present study Pr and Sc are of order 1, therefore, $\tilde{Pr}$ and $\tilde{Sc}$ are taken to be 1. This means that the effects of interfacial waves on the heat and mass transfer are identical to the momentum transfer.

4. SOLUTION METHOD

In view of the impossibility of obtaining an analytic solution for the non-linear coupling differential equations, the conjugated problem defined by the governing equations, equations (1)–(6), is solved by the finite-difference numerical method. In the present study, the matching conditions imposed at the gas–liquid interface, equations (14) and (16), to ensure the continuities of shear stress and heat flux are cast in backward difference for $(\partial\phi/\partial y)_g$ and forward difference for $(\partial\phi/\partial y)_l$ with ϕ denoting u or T. Therefore, the governing equations in the gas flow and liquid film can be solved simultaneously.

Because the flow under consideration is a boundary-layer type, the solution for equations (1)–(6) can be marched in the downward direction. A fully implicit numerical scheme in which the axial convection terms are approximated by the upwind difference and the transverse convection and diffusion terms by the central difference is employed to transform the governing equations into finite-difference equations. Each system of the finite-difference equations forms a tridiagonal matrix equation which can be efficiently solved by the Thomas algorithm [16]. For a given condition, a brief outline of the solution procedures is described as follows:

(1) Guess an inlet velocity u_o.

(2) For any axial location, guess the values of (dp_m/dx) and δ by the Newton–Raphson method [17], and solve the finite-difference forms of equations (1)–(6) for u, θ, and w.

(3) Integrating the continuity equation of the gas stream numerically to find v

$$v = -\frac{1}{\rho}\frac{\partial}{\partial x}\int_0^y \rho u \, dy. \tag{25}$$

(4) Check the satisfaction of the overall conservation of mass in the gas flow and liquid film. If the following criteria

$$\left|\int_0^{b-\delta} \rho u \, dy - \left[\rho u_o (b-\delta_o) + \int_0^x \dot{m}_l'' \, dx\right]\right| \Big/ \rho u_o b < 10^{-4} \tag{26a}$$

and

$$\left|B - \left[\int_{b-\delta}^{b} (\rho u \, dy)_l + \int_0^x \dot{m}_l'' \, dx\right]\right| \Big/ B < 10^{-4} \tag{26b}$$

are met, then test the convergence of the velocity, temperature, and concentration fields. If the maximum relative errors for u, T, and w between two consecutive iterations satisfy the criteria

$$\frac{\max|u_{i,j}^n - u_{i,j}^{n-1}|}{\max|u_{i,j}^n|} < 10^{-4} \tag{27a}$$

$$\frac{\max|T_{i,j}^n - T_{i,j}^{n-1}|}{\max|T_{i,j}^n|} < 10^{-4} \tag{27b}$$

$$\frac{\max|w_{i,j}^n - w_{i,j}^n|}{\max|w_{i,j}^n|} < 10^{-4} \tag{27c}$$

the solution for the current axial location is complete. Now if equations (27) are not simultaneously met, repeatedly solve the finite-difference equations for u, T, and w in the gas stream and liquid film and use equation (25) to get v until the condition specified in equations (27) is fulfilled. If equations (26) are not satisfied, adjust dp_m/dx, $\dot{m}_l''$ and δ and repeat procedures (2)–(4) for the current axial location.

(5) Procedures (2)–(4) are successively applied to every axial location from the channel entrance to exit.

(6) Check whether the exit pressure p_m is zero. If not, guess a new inlet velocity u_o by the Newton–Raphson method and repeat procedures (2)–(6). If yes, the solution is complete.

One point worth mentioning is that both the magnitude and shape of the inlet velocity u_o are not known before the complete solution for the governing equations, including the inlet and exit effects, is obtained [10, 18]. In refs. [9, 10], it was shown that the shape

Table 1. Comparison of local interfacial heat flux q_l'' for various grid arrangements for the case with $T_{li} = T_o = 30°C$ and $B = 0.02$ kg m^{-1} s^{-1}

x/l	$I \times J \times L$				
	$201 \times 161 \times 41$	$101 \times 161 \times 21$	$101 \times 81 \times 21$	$51 \times 81 \times 11$	$51 \times 41 \times 11$
0.047	791.20	777.11	795.56	804.48	849.43
0.1026	506.11	497.62	513.01	501.08	523.93
0.2005	342.16	337.52	345.14	333.51	349.88
0.4086	224.32	215.50	218.25	214.62	227.95
0.6521	163.20	156.74	157.37	156.32	165.40
0.9117	127.87	128.59	128.96	125.04	128.25

I, total number of grid points in the x-direction.
J, total number of grid points placed in the y-direction in the gas side.
L, total number of grid points placed in the y-direction in the liquid side.

of u_o has little effect on the heat and mass transfer in the flow. Thus, in the present study u_o is assumed to be uniform. Note that the thickness of the liquid film decreases with x due to the film evaporation. Therefore, during the downward marching at each iteration the numerical grid is rearranged to ensure that one of the grid points is located at the gas–liquid interface.

To obtain enhanced accuracy in the numerical computations, grids are chosen to be nonuniform in the streamwise direction and in the transverse direction to account for the drastic variations of u, T, and w in the regions near the inlet and gas–liquid interface. Several grid sizes are tested and a comparison of the results among the computations for a typical case is given in Table 1. It is noted that the difference in the local interfacial heat flux, q_l'', for the computation by using the $101 \times 81 \times 21$ and $201 \times 161 \times 41$ grids is always less than 4%. Accordingly, the computation by the $101 \times 81 \times 21$ grid is sufficient to understand the heat and mass transfer characteristics in the gas flow and liquid film. To further check the adequacy of the numerical scheme, the results for the limiting case of natural convection in a vertical channel without the film evaporation under asymmetric wall temperatures are obtained. Excellent agreement between the present predictions and those of Aung *et al.* [19] was found.

5. RESULTS AND DISCUSSION

As mentioned in refs. [4, 5], the governing dimensionless parameters, Gr_T, Gr_M, Pr and Sc, are interdependent and cannot be arbitrarily assigned. Instead, in this study the physical parameters—the inlet liquid temperature T_{li}, inlet liquid mass flow rate B, ambient temperature T_o, channel width $2b$ and channel length l—are picked as the independent variables. The ranges of each parameter for the analysis are listed in Table 2. Notice that in Table 2, the ambient temperatures are different case by case. The reason of this choice is to facilitate the comparison between the predictions and measured data. Hence, the same experimental condition [3] is employed as the input data for the numerical simulation in each numerical run.

Because ethanol is considered for the liquid film, the direction of the solutal buoyancy B_M would act downwards due to the larger molecular weight for ethanol vapour than air. As for the thermal buoyancy B_T, the direction depends on whether the temperature of the gas stream is higher than that of the ambient or not. Therefore, the induced flow in the channel may move upwards or downwards, depending on the direction of the resultant forces of combined thermal and solutal buoyancy forces along with the interfacial shear force acted by the falling film. During the experimental measurement [3, 4], the smoke was injected into the vertical channel. It was found that the induced flow moves in the downward direction for all cases listed in Table 2. With the boundary-layer approximations adopted, the problem, therefore, can be solved by the boundary-layer type governing equations.

Shown in Figs. 2–4 are the predicted axial developments of velocity, temperature and mass fraction of ethanol vapour. For clear illustration, the velocity and temperature distributions in the region close to the interface are inserted in the figures. Due to the space limit, only the results for $T_{li} = 40$ and 30°C at $B = 0.02$ kg m^{-1} s^{-1} are presented. One point worth mentioning is that in the present numerical simulation the mass fraction of ethanol vapour at the ambient is assumed to be zero. An overall inspection of Fig. 2 discloses that the velocity of the gas stream near the channel entrance is relatively uniform. As the flow moves downstream, the profile becomes distorted

Table 2. The ranges of the physical parameters

Inlet liquid temperature, T_{li} (°C)	$27 \sim 40$
Inlet liquid mass flow rate, B (kg m^{-1} s^{-1})	$0.01 \sim 0.04$
Ambient temperature, T_o (°C)	$T_o = 31.5$°C as $T_{li} = 40$°C $T_o = 30$°C as $T_{li} = 30$°C $T_o = 30.5$°C as $T_{li} = 27$°C
Channel width, $2b$ (m)	0.03
Channel length, l (m)	1.0

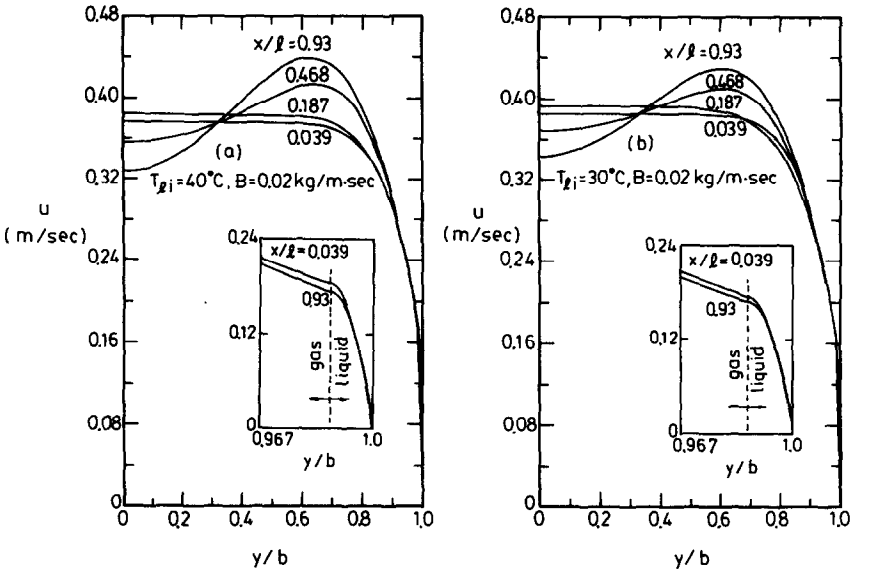

FIG. 2. Developments of axial velocity profiles.

with the maximum velocity shifting away from the centreline of the channel. This feature is the direct consequence of the fact that the combined action of the thermal buoyancy B_T, solutal buoyancy B_M and interfacial shearing force accelerates the gas near the interface, and meanwhile the gas in the core region decelerates to maintain the overall mass balance. It is clearly seen in the inserted plots that the liquid slightly decelerates in the downward direction. This apparently results from the continuous evaporative cooling of the liquid film and the associated increase of its viscosity as it falls down.

Figure 3 presents the axial developments of temperature for the cases with $T_{li} = 40$ and 30°C at $B = 0.02$ kg m^{-1} s^{-1}. Drastic variations of temperature profiles are found in Fig. 3(a) for $T_{li} = 40$°C. In order to understand these complex variations, attention is first paid to examining the temperature profiles near the gas–liquid interface in the inserted plot. Near the entrance (e.g. $x/l = 0.039$ and 0.187), the gas and liquid temperatures at a given x increase monotonically with y up to the channel wall. Apparently, the directions of sensible heat transfer in the gas flow and liquid film are the same, and are from the interface to the gas stream and from the wall to the interface. The energy loss during the decrease in the liquid film temperature with x is used to supply the energy needed for the sensible and latent heat exchanges

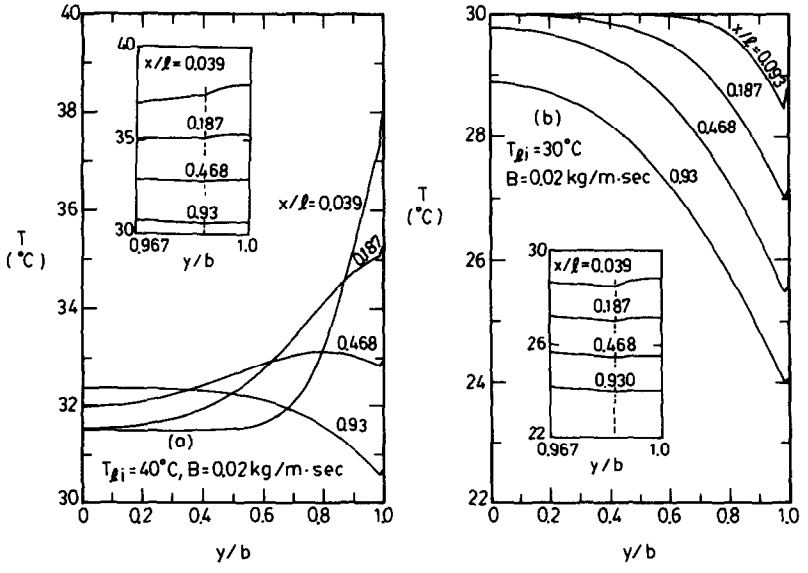

FIG. 3. Developments of axial temperature profiles.

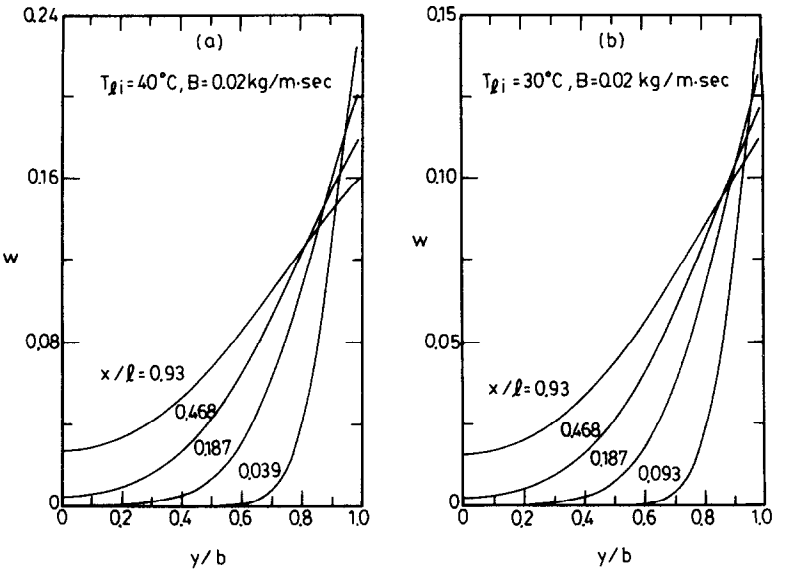

FIG. 4. Developments of axial mass-fraction profiles.

at the interface. As the liquid film moves downstream, as indicated in the inserted plot in Fig. 3(a) ($x/l = 0.468$ and 0.93), the gas temperature near the interface decreases with y down to the gas–liquid interface and the temperature then increases with y in the liquid side. This indicates that the sensible heat transfer in the gas side and liquid film all goes to the interface and is absorbed during the film vaporization, a latent heat transfer process. The energy absorption by the film vaporization is so effective that the gas and liquid near the interface at $z/l = 0.93$ are below the ambient temperature ($T_o = 31.5°C$). Although the gas temperature near the interface decreases with x, the temperature in the core of the channel increases gradually with x.

Attention is turned to Fig. 3(b) in which T_{li} is kept at 30°C, equal to T_o. It is apparent in Fig. 3(b) that the temperature in the gas flow and liquid film decreases monotonically with x. Notice that in the inserted plot in Fig. 3(b) the gas temperature at a given x decreases with y down to the gas–liquid interface, indicating that the direction of interfacial sensible heat transfer in the gas side is from the gas to interface. The liquid temperature, however, increases with y. This suggests that heat transfer in the liquid film is from the liquid to the interface although $T_o \geqslant T_I$. From the above results, the following conclusion can be drawn: for the cases with $T_o \geqslant T_{li}$, the energy needed to sustain the film evaporation, a latent heat transfer process, is provided from the sensible heat transfer in the gas flow and liquid film. It is important to point out that from examining the inserted plots in Fig. 3, at a given axial location the temperature in the liquid film is relatively uniform because the film is rather thin.

Figure 4 displays the axial developments of the mass fraction of ethanol vapour. In line with the evaporation of the ethanol film, the mass fraction of ethanol vapour in the gas flow in the central portion of the channel increases gradually as the air moves downstream. Higher concentration of ethanol vapour is found for the case with $T_{li} = 40°C$. This is a direct consequence of a larger amount of ethanol vapour entering the air stream for the case with a higher T_{li}. Due to the evaporative cooling, the interfacial temperature decreases along the channel. Therefore, the corresponding mass fraction of ethanol vapour near the gas–liquid interface then decreases with x, as shown in Fig. 4. This feature is also clearly illustrated in Fig. 5 where the axial distributions of interfacial temperature and mass fraction are presented for various cases. In Fig. 5, because of the larger total internal

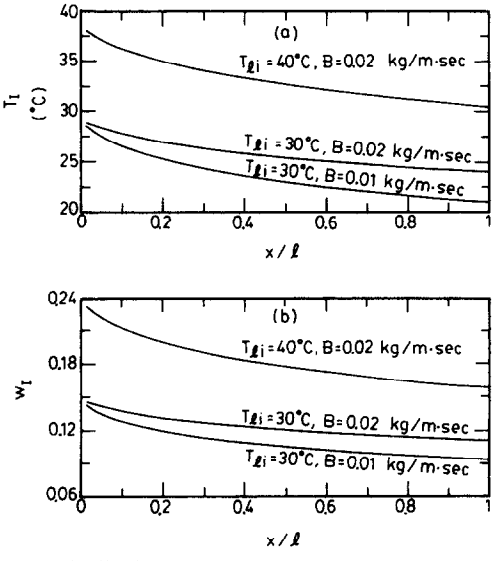

FIG. 5. Distributions of axial interfacial temperature and mass fraction.

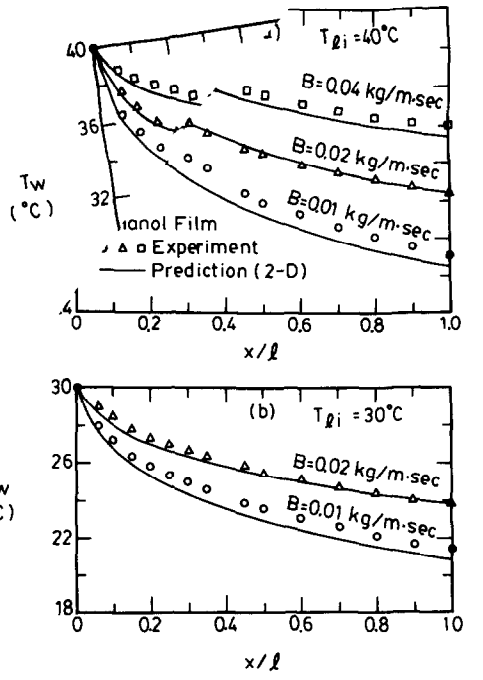

FIG. 6. Local temperature distributions along the insulated channel wall.

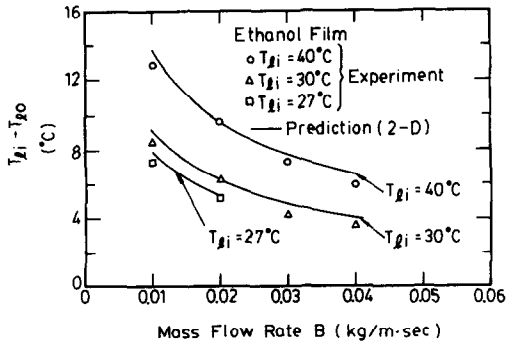

FIG. 7. Effects of liquid mass flow rate on the temperature drops.

energy (i.e. larger $Bc_p\Delta T_l$) for the liquid film with larger B, a higher interfacial temperature is found for these cases.

Figure 6 shows the predicted axial distributions of the liquid film temperature at the insulated wall. For comparison purposes, the experimental data from ref. [3] are also included in this figure. The upper plot corresponds to the results for $T_{li} = 40°C$ and $T_o = 31.5°C$ while the lower is for $T_{li} = T_o = 30°C$ at different B. Basically, the predicted results agree well with the experimental data for each case. Careful scrutiny of Fig. 6 indicates that the wall temperature is slightly underpredicted in some cases. This may be due to the fact that in the numerical simulation the mass fraction of the ethanol vapour at the ambient, w_o, is assumed to be zero. But in reality, the condition of mass fraction at ambient is difficult to keep at $w_o = 0$ during the experiment. In the separate numerical computation, the effect of w_o was also tested. It was found that the predicted results are improved by comparing with the experimental data when w_o was chosen to be slightly above zero.

In the study of evaporative cooling, the total temperature drop of the liquid film as it flows from the inlet to the outlet is one of the important quantities. For this reason, the total temperature drop of the liquid film is presented in Fig. 7 for different conditions. It is apparent in this plot that the temperature drop is only slightly overpredicted for some cases. Note that the higher the T_{li}, the larger the total temperature drop. This is due to the effective evaporative cooling for the case with a high T_{li}. In addition, the larger temperature depression is also found for the case with a smaller liquid mass flow rate.

To demonstrate the relative importance of the sensible and latent heat exchanges between the gas–liquid interface and gas flow, three kinds of interfacial heat fluxes from the predictions are illustrated in Fig. 8. Regarding the curves for the interfacial sensible heat transfer in the gas side q''_{sl}, substantial differences exist among various cases. The positive value of q''_{sl} indicates that the direction of sensible heat transfer is from the interface to the gas stream, vice versa for a negative q''_{sl}. For the curve with $T_{li} = 40°C$ and $B = 0.02$ kg m^{-1} s^{-1}, q''_{sl} is positive at the initial entrance ($x/l < 0.26$). But as the flow goes downstream, q''_{sl} gradually decreases and finally becomes negative. This can be made plausible by

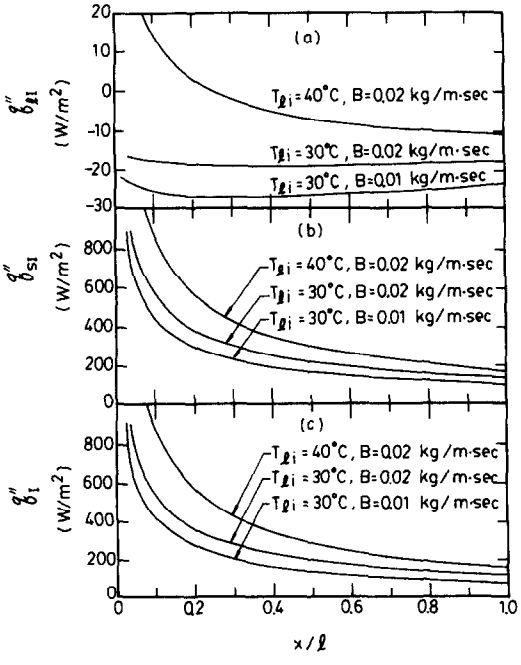

FIG. 8. Distributions of local heat transfer rates in the gas side along the channel: (a) interfacial sensible heat transfer; (b) interfacial latent heat transfer; (c) total interfacial heat transfer.

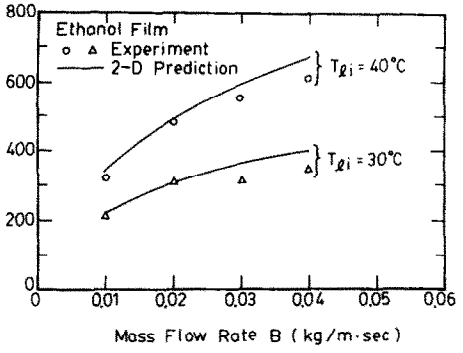

FIG. 9. Effects of liquid mass flow rate on the average interfacial heat transfer rates.

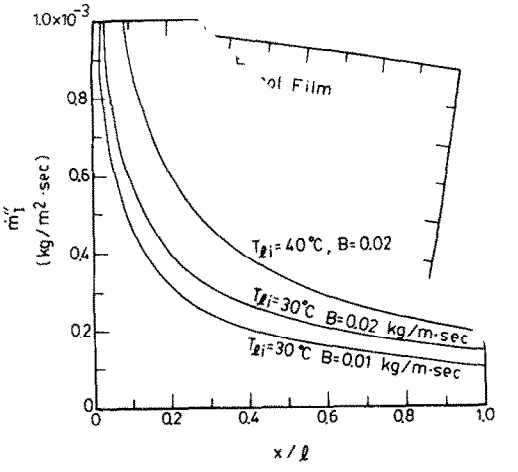

FIG. 10. Local interfacial mass evaporation rate along the channel.

checking the results in Fig. 3. In that figure the interface temperature in the entrance region is above the gas temperature, the interfacial sensible heat flux is, therefore, from the interface to the gas stream, indicating a positive q_{sI}''. But as the liquid moves further downstream, because of the strong evaporative cooling, T_I falls below the gas temperature at a certain axial location. Hence, the direction of interfacial sensible heat transfer reverses. As for the curves with $T_{Ii} = T_o = 30°C$, q_{sI}'' is always negative. This is simply due to the fact that the interface temperature is always below the gas temperature.

Attention is now turned to the distributions of the interfacial latent heat transfer q_{lI}'' (see Fig. 8(b)). According to the results in Fig. 8(b), at a given B the system with a higher inlet liquid temperature shows a larger value for q_{lI}''. This is brought about by the larger latent heat transport in connection with the larger liquid film evaporation for a higher T_{Ii}. The results given in Fig. 8(b) also show that larger q_{lI}'' results for the system with a larger B. This is again due to the larger latent heat transfer for the system with a larger B, i.e. a larger interfacial liquid film temperature, as clear in Fig. 5. It becomes apparent, by checking the magnitudes of q_{sI}'' and q_{lI}'', that in the gas side heat transfer resulting from the latent heat exchange is much more effective. Shown in Fig. 8(c) are the local distributions of the total interfacial heat flux q_I'' (i.e. $q_I'' = q_{sI}'' + q_{lI}''$). The value of q_I'' is always positive, indicating that the direction of the total interfacial heat transfer is from the interface to the gas stream.

Figure 9 displays the results of the average interfacial heat flux for different conditions. For comparison purposes, the experimental data from ref. [3] are also plotted in this figure. In this plot, the measured $\overline{q_I''}$ is estimated by the equation

$$\overline{q_I''} = Bc_{pl}(T_{Ii} - T_{Io})/l \tag{28}$$

where T_{Ii} and T_{Io} are, respectively, the measured inlet and exit liquid film temperatures. At low liquid mass flow rate, the predictions agree well with the experimental results. As for high liquid mass flow rate, the differences between the numerical predictions and experimental data become large and are about 10%. Also clearly shown in Fig. 9 is that larger q_I'' is experienced for the case with a larger B. This results from the larger interfacial liquid film temperature for the case with larger B, which in turn, causes a larger evaporative latent heat transfer. Moreover, larger $\overline{q_I''}$ is found for the system with a higher T_{Ii}.

Depicted in Fig. 10 are the predicted axial distributions of the mass evaporation rate at the gas–liquid interface. The results indicate that larger mass evaporation rate is found for the case with $T_{Ii} = 40°C$. This confirms the fact that film evaporation is much more effective for the system with a higher T_{Ii}. Also found in this plot is the influence of the inlet liquid mass flow rate B on the mass evaporation rate. Results show that the larger the liquid flow rate, the larger the mass evaporation rate.

The amount of ethanol vapour added to the gas stream due to film vaporization is important in improving our understanding of the heat and mass transfer effect. To this end, a non-dimensional accumulated mass evaporation rate is introduced

$$M_r = \frac{\text{evaporating mass flow rate}}{\text{inlet liquid mass flow rate}} = \int_0^x \dot{m}_l'' \, dx/B. \tag{29}$$

The distributions of M_r for various cases are illustrated in Fig. 11. It is clearly seen in this plot that larger film evaporation is observed for the system with a higher T_{Ii} or smaller B. One point worth mentioning is that the dimensionless accumulated mass evaporation rate at $x/l = 1$ is always less than 4%.

6. CONCLUSIONS

The nature of laminar natural convection heat and mass transfer in vertical plate channel flows with film evaporation has been numerically studied. The effects

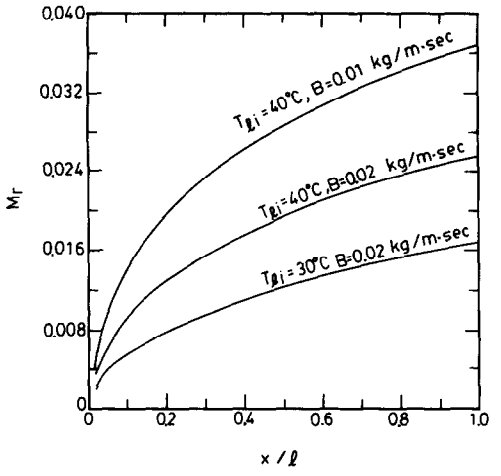

FIG. 11. Distributions of the dimensionless accumulated evaporation rate.

of the system temperature and inlet liquid mass flow rate on the momentum, heat and mass transfer in the gas flow and liquid film are examined in great detail. What follows is a brief summary of the major results:

(1) Heat transfer in the gas side is dominated by the transport of latent heat in association with the evaporation of the liquid film.

(2) The influences of the evaporative latent heat transfer on the cooling of the liquid film depend largely on the inlet liquid film temperature T_{li} and inlet liquid mass flow rate B. Results show that the higher (smaller) the $T_{li}(B)$, the larger the liquid film cooling.

(3) The predictions agree well with the experimental data from ref. [3].

(4) Due to strong evaporative cooling of the ethanol film, the outlet temperature along the channel could drop below the ambient temperature in spite of the inlet film temperature being above the ambient temperature.

Acknowledgement—The financial support of this research by the engineering division of National Science Council of Taiwan, R.O.C., through contract NSC77-0401-E009-10 is greatly appreciated.

REFERENCES

1. S. Oktay, R. Hannemann and B. C. Avran, High heat from a small package, *Mech. Engng* 34–42 (March 1986).
2. R. O. Chu, Heat transfer in electronic system, *Proc. 8th Int. Heat Transfer Conf.*, San Francisco, Vol. 1, pp. 293–305 (1986).
3. W. M. Yan, T. F. Lin and Y. L. Tsay, Evaporative cooling of liquid film through interfacial heat and mass transfer in a vertical channel—I. Experimental study, *Int. J. Heat Mass Transfer* **34,** 1105–1111 (1991).
4. W. M. Yan, Buoyancy induced heat and mass transfer in vertical channel flows, Ph.D. Thesis, Department of Mechanical Engineering, National Chiao Tung University, Hsinchu, Taiwan, January (1989).
5. C. J. Chang, T. F. Lin and W. M. Yan, Natural convection flows in a vertical open tube resulting from combined buoyancy effects of thermal and mass diffusion, *Int. J. Heat Mass Transfer* **29,** 1453–1552 (1986).
6. W. W. Baumann and F. Thiele, Heat and mass transfer in two-component film evaporation in a vertical tube, *Proc. 8th Int. Heat Transfer Conf.*, San Francisco, Vol. 4, pp. 1843–1848 (1986).
7. T. R. Shembharkar and B. R. Pai, Prediction of film cooling with a liquid coolant, *Int. J. Heat Mass Transfer* **29,** 899–908 (1986).
8. JSME Data: Thermophysical Properties of Fluids, The Japan Society of Mechanical Engineers (1983).
9. T. Aihara, Effects of inlet-condition on numerical solution of free convection between vertical parallel plates, Report No. 258, Institute of High Speed Mechanics, Tohoku University, Sendai, Japan (1973).
10. C. Chang and T. F. Lin, Natural convection in heated vertical channel including entrance and exit effects, *Proc. 3rd Int. Symp. on Transport Phenomena in Thermal Control*, Taipei, Taiwan, 14–18 August, pp. 521–532 (1988).
11. A. E. Dukler, Characterization, effects and modeling of the wavy interface, *Prog. Heat Mass Transfer* **6,** 207–234 (1972).
12. K. Suzuki, Y. Hagiwara and T. Sato, Heat transfer and flow characteristics of two-component annular flow, *Int. J. Heat Mass Transfer* **26,** 597–605 (1983).
13. R. I. Hirshburg and L. W. Florschuetz, Laminar wavy-film flow: Part I, hydrodynamic analysis, *J. Heat Transfer* **104,** 452–458 (1982).
14. C. Massot, F. Iraani and E. N. Lightfoot, Modified description of wave motion in a falling film, *A.I.Ch.E. Jl* **12,** 445–455 (1966).
15. A. Gollan and S. Sideman, On the wave characteristics of falling films, *A.I.Ch.E. Jl* **15,** 301–303 (1969).
16. S. V. Patankar, *Numerical Heat Transfer and Fluid Flow*, Chap. 6. Hemisphere/McGraw-Hill, New York (1980).
17. D. A. Anderson, J. C. Tannehill and R. H. Pletcher, *Computational Fluid Mechanics and Heat Transfer*, Chap. 7. Hemisphere/McGraw-Hill, New York (1984).
18. T. F. Lin, Heat transfer enhancement through latent heat transfer in natural convection—III, Report No. NSC-77-0401-E009-10, Taiwan (1989).
19. W. Aung, L. S. Fletcher and V. Sernas, Developing laminar free convection between vertical flat plates with asymmetric heating, *Int. J. Heat Mass Transfer* **15,** 2293–2308 (1972).

REFROIDISSEMENT EVAPORATIF D'UN FILM LIQUIDE PAR TRANSFERT INTERFACIAL DE CHALEUR ET DE MASSE DANS UN CANAL VERTICAL—II. ETUDE NUMERIQUE

Résumé—Une étude numérique est conduite sur le refroidissement d'un film liquide tombant par transfert de chaleur et de masse à l'interface vers un écoulement de convection naturelle. Les résultats présentés correspondent à l'évaporation d'un film d'éthanol. Les résultats du calcul sont comparés aux résultats expérimentaux. Les prédictions montrent que les effets du transfert évaporatif de chaleur latente sur le refroidissement du film liquide dépendent beaucoup de la température d'entrée du film et de son débit-masse. De plus le transfert de chaleur depuis l'interface vers l'écoulement de gaz est principalement lié au transport de chaleur latente en conjonction avec l'évaporation du film liquide.

VERDUNSTUNGSKÜHLUNG EINES FLÜSSIGKEITSFILMS IN EINEM SENKRECHTEN KANAL DURCH WÄRME- UND STOFFTRANSPORT AN DER GRENZFLÄCHE—II. NUMERISCHE UNTERSUCHUNG

Zusammenfassung—Die Verdunstungskühlung eines Rieselfilms durch Wärme- und Stofftransport an der Grenzfläche in Kanalströmungen bei freier Konvektion wird numerisch untersucht. Für das System eines verdunstenden Ethanolfilms werden Wärme- und Stoffübergangskoeffizienten vorgestellt. Die berechneten Ergebnisse werden experimentellen Werten gegenübergestellt. Die Berechnungen zeigen, daß der Einfluß des Transports latenter Verdunstungswärme auf die Kühlung des Flüssigkeitsfilms stark von der Eintrittstemperatur und der Massenstromdichte der Flüssigkeit abhängt. Darüberhinaus zeigen die Ergebnisse, daß der insgesamt über die Grenzfläche an den Gasstrom übertragene Wärmestrom von den gekoppelten Vorgängen des Transports latenter Wärme und der Verdunstung des Flüssigkeitsfilms dominiert wird.

ИСПАРИТЕЛЬНОЕ ОХЛАЖДЕНИЕ ЖИДКОЙ ПЛЕНКИ ПРИ ТЕПЛО- И МАССОПЕРЕНОСЕ НА ГРАНИЦЕ РАЗДЕЛА В ВЕРТИКАЛЬНОМ КАНАЛЕ—II. ЧИСЛЕННОЕ ИССЛЕДОВАНИЕ

Аннотация—Проводится численный анализ испарительного охлаждения стекающей жидкой пленки при тепло- и массопереносе на границе раздела в условиях естественноконвективных течений в канале. В частности, представлены результаты расчета скоростей тепло- и массопереноса для систем с пленочным испарением этанола. Результаты расчетов сравниваются с экспериментальными данными. Расчеты показывают, что влияние скрытой теплоты парообразования на охлаждение жидкой пленки в значительной мере зависит от температуры жидкой пленки на входе и массового расхода жидкости. Кроме того, полученные результаты свидетельствуют о том, что теплоперенос от границы раздела к потоку газа определяется испарением жидкой пленки.